Contents list available at IJRED website

International Journal of Renewable Energy Development

Journal homepage: https://ijred.undip.ac.id

Research Article

Agricultural waste-based magnetic biochar produced via hydrothermal route for petroleum spills adsorption

Dessy Ariyanti[a,b*], I Nyoman Widiasa[a], Marissa Widiyanti[a], Dina Lesdantina[a,b], Wei Gao[c]

[a]*Department of Chemical Engineering, Faculty of Engineering, Universitas Diponegoro, Tembalang, Semarang, Indonesia*

[b]*SDGs Center, Universitas Diponegoro, Tembalang, Semarang, Indonesia*

[c]*Department of Chemical and Materials Engineering, the University of Auckland, Auckland, New Zealand*

Abstract. Oil spills are one of the marine pollution events triggered by the results of tanker operations (air ballast), ship repairs and maintenance (docking), mid-ocean loading and unloading terminals, air bilge (drainage of water, oil, and engine-processed lubricants), ship scrapping, and the most common accidents/collisions of tankers. The impacts vary from the death of marine organisms, especially fish, changes in reproduction and behavior of organisms, plankton contamination, fish migration, as well as ecosystem damage, and economic loss. Bio-based absorbents such as biochar can be an environmentally friendly alternative to chemical sorbents that works to adsorb oil spills faster. In this study, the effectiveness of magnetic biochar in oil spill removal was investigated. It also includes the synthesisation of magnetic biochar from agricultural waste (bagasse, rice husks, and sawdust) using the hydrothermal method at a temperature of 200°C. Hydrothermal carbonization is considered a cost-effective method for biochar production because the process can be carried out at low temperatures around 180°- 250°C. Biochar characterization was carried out with a Scanning Electron Microscope and Energy Dispersive X-Ray (SEM-EDX), Fourier Transform Infrared Spectroscopy (FTIR), and X-Ray Diffraction (XRD)**.** The Brunauer, Emmett, and Teller (BET) and Barrett–Joyner–Halenda (BJH) were used to analyse the surface area and pore size distribution. Based on the results of the SEM-EDX analysis, only biochar was made from rice husk and sugarcane bagasse which contained Fe elements, as a result of the $FeCl_3.6H_2O$ reaction. This condition is also proven by the presence of the FeO on both samples based on FTIR. The three synthesized biochar are amorphous and categorized as mesopores due to pore size around 15 to 16 nm, which can absorb petroleum spills with a percentage of 81% for sugarcane bagasse-based biochar, 84% for rice husk-based biochar, and 70% for sawdust-based biochar. Biochar from rice husk has excellent adsorption effectiveness with an adsorption capacity of 0.21 g/g in 60 min due to its large functional group area and the excellent attachment of magnetic compound into the biochar surface to form magnetic biochar.

Keywords: biochar, oil spills, hydrothermal, adsorption, agricultural waste

@ The author(s). Published by CBIORE. This is an open access article under the CC BY-SA license (http://creativecommons.org/licenses/by-sa/4.0/).

Received: 31st January 2023; Revised: 2nd March 2023; Accepted: 27th March 2023; Available online: 7th April 2023

1. Introduction

Oil spills are one of the marine pollution incidents that can be caused by the results of tanker ship operations (ballast water), ship repair and maintenance (docking), mid-sea loading and unloading terminals, bilge water (water drains, oil and engine-processed lubricants), scrapping ships, and the event often occurs is a tanker accident/collision. Oil spills have long-term accumulation impacts that are harmful to life in the sea, sea coasts, and marine ecosystems. The impacts vary, ranging from the death of marine organisms, especially fish, changes in reproduction and behavior of organisms, plankton contamination, fish migration, ecosystem damage, and economic losses (AlAmeri *et al.*, 2019; KKP, 2022; Madhubashani *et al.*, 2021). For cases of oil spills in open waters, the concentration of oil under slick is usually very low, and the maximum will be in the range of 0.1 ppm so as not to cause mass death of organisms, especially fish. The problem is, most cases of oil spills occur in coastal waters or deep waters (B. Zhang *et al.*, 2018). Laboratory tests have shown that the reproduction and behavior of fish and shellfish organisms are affected by the concentration of oil in the water. This hazardous waste will directly impact on organisms, especially when they are still in the egg and larval phases (Helle *et al.*, 2020; Yuewen & Adzigbli, 2018). It will be even worse when the location affected by the oil spill is a closed/semi-enclosed area such as a polluted bay (Honda & Suzuki, 2020; Singh *et al.*, 2020). Coastal and marine ecosystems (mangroves, river deltas, estuaries, sea grasses, and coral reefs) have ecologically important functions and roles (Duke, 2016). The entry of hazardous and toxic waste into coastal waters can disrupt ecosystems, because the coastal area is a breeding area, providing habitat and food for adult organisms or other habitats around it. Data from International Tanker Owners Pollution Federation Limited (ITOPF) shows that 6 oil spills of more than 7 tons were recorded as coming from tanker accidents. This condition improved slightly in 2020, but was comparable to the average in 2010. Large-scale oil spill incidents (over 700 tons) occurred in Asia in April 2021, including heavy crude oil. While the others are classified as medium-scale oil spill incidents, which include crude, slurry,

* Corresponding author
Email: dessy.ariyanti@che.undip.ac.id (D.Ariyanti)

https://doi.org/10.14710/ijred.2023.52180
ISSN: 2252-4940/© 2023.The Author(s). Published by CBIORE

and non-persistent oils. The total volume of oil lost to tanker spills in 2020 is 10,000 tons, most of which were spilled in one major incident. This figure is higher than the previous two years (ITOPF, 2022). The data shows that from 2016 to early 2022 there were eight oil spill accidents in Indonesian waters (Institute, 2022) and forty-three accidents in the world.

Petroleum or crude oil is a mixture of several hydrocarbons, including polycyclic aromatic hydrocarbons and alkanes. Oil spill clean-up can be carried out using mechanical, chemical, or biological methods (Yi *et al*., 2020). The selection of an effective method is based on the amount and type of crude oil spilled (heavy or light), the location, and the cost of the spill. Although the mechanical method is widely used, it is expensive and requires special equipment. The biological approach is quite slow and requires more than one type of microorganism to degrade all organic compounds in an oil spill. Chemical dispersants are effective enough to remove up to 90% of crude oil spills (Graham *et al*., 2010). The use of chemical dispersants is quite large and they can harm marine ecosystems ((El Gheriany *et al*., 2020; Madhubashani *et al*., 2021; Rajabi *et al*., 2021; Tao *et al*., 2019).

Remediation of crude oil spills by adsorption method has developed in recent years (Piperopoulos *et al*., 2020). Various types of hydrophobic absorbents such as cellulose aerogels, polyurethane sponges, poly(alkoxysilane) organo-gels, graphene-wrapped sponges, micro fibrillated cellulose, Fe_3O_4/magnetic polystyrene nanoparticles have been investigated for their potential use for cleaning up crude oil spills (Sabir, 2015; Subrati *et al*., 2017). These materials generally have pore characteristics and can bind various types of oil by surface adsorption and adsorption in the pores. Bio-based adsorbents such as biochar can be an environmentally friendly alternative to chemical sorbents due to their high adsorption capacity and biodegradation potential (AlAmeri *et al*., 2019; Cai *et al*., 2019; Duan *et al*., 2021; Gurav *et al*., 2021; Tao *et al*., 2019; Wei *et al*., 2020).

Generally, pyrolysis is the most common technique for synthesizing biochar, at high temperatures (> 400°C) in the absence of oxygen (Leng & Huang, 2018; Li *et al*., 2017). Ahmed *et al*. conducted an experiment to synthesize biochar using sawdust from the furniture industry by pyrolysis with a temperature range of 400 - 600°C with maintaining the nitrogen flow rate (Ahmed *et al*., 2020). Biochar derived from pine needles was also produced through pyrolysis process up to 800°C under oxygen-limited conditions (Ouyang *et al*., 2019). However, all of these processes is categorized as high energy consumption process. Meanwhile, there are other technique such as hydrothermal carbonization that is considered a cost-effective method for biochar production because the process can be carried out at low temperatures around 180° - 250°C (Cai *et al*., 2019; Yaashikaa *et al*., 2020). The studies related to the hydrothermal production of biochar include Wu *et al*, who developed biochar from agricultural waste cassava slag by simple hydro-thermal carbonization treatment for Rhodamine B adsorption. The produced biochar possessed maximum biochar adsorption capacity of 105.3 mg/g (Wu *et al*., 2020). While Zhang et. al conducted an experiment to synthesize biochar and magnetic biochar from biosolids by the hydrothermal process to test the use of magnetic biochar as a support matrix for enzyme immobilization. The results show that magnetic biochar has the same surface area as biochar, but performs better as a support matrix (H. Zhang & Hay, 2020). Almost all the research related to the synthesis of biochar uses various kinds of raw materials and different applications. In this paper the synthetization of biochar from various agricultural waste biomass (bagasse, rice husk, and sawdust) using the hydrothermal method were investigated, and its application as an adsorbent for petroleum spills were studied. This paper emphasized the use of hydrothermal method for magnetic biochar production for energy efficient technology in comparison to pyrolysis and the application of magnetic biochar from agricultural waste biomass for the adsorption of oil spills has not been widely carried out.

2. Materials and Methods

2.1 Materials

Several materials were prepared including raw materials and reagents. Raw materials for biochar production used in this experiment originated from agricultural waste biomass such as sugarcane bagasse, rice husk, and sawdust which was purchased from traditional markets in Semarang, Indonesia. Biomass that has been purchased was re-selected to obtain material that is still in good condition and separated from its impurities. The biomass was then floured and dried in an oven at 80°C for 24 hours and stored in a desiccator until it was used for maintaining its consistency. Other chemicals such as hexamethyl diamine (HDA) (Merck) and $FeCl_3.6H_2O$ (Merck) was used in the synthesis biochar. The reagents needed for adsorption analysis are NaCl (Merck), KCl (Merck) and also distilled water. Apart from making synthetic seawater, distilled water is needed for product washing. All chemical reagents used for hydrothermal processes and adsorption analysis were analytical grade and used without prior treatment. These chemicals were purchased through P.T. Merck Chemicals and Life Sciences as affiliated Merck KGaA, Darmstadt, Germany. The hydrothermal process conducted in this experiment is carried out in the Teflon-linked autoclaves as reactors. In addition, an orbital shaker was used to analyze the performance of biochar in adsorbing petroleum spills. Both tools are presented in Fig. 1.

2.2 Experimental Procedures

2.2.1 Magnetic Biochar Synthesis

Biochar from raw material sugarcane bagasse, rice husk, and sawdust was synthesized by hydrothermal method. The process in general consists of three stages including the mixing of raw material with other reagents, the hydrothermal process, and the last stage that consist of washing, filtering and drying. First, 4.5 g of prepared biomass was dispersed into 70 mL of distilled water, then 2.8 g of hexamethyl diamine (HDA) and 2.7 g of $FeCl_3.6H_2O$ were added to the mixture. The mixture then stirred at 250 rpm at atmospheric temperature for 20 minutes. After that, the suspension was poured into 100 mL Teflon-linked autoclave and put in the oven to be processed with the hydrothermal method at a temperature of 200°C for 24 hours.

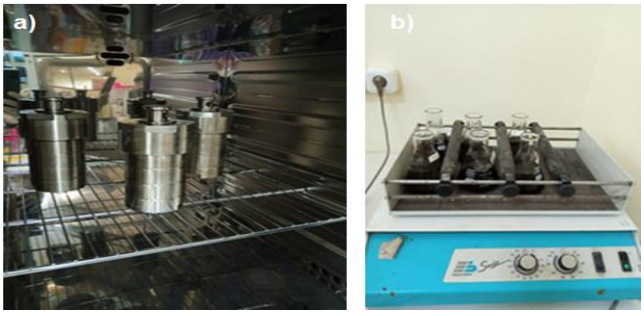

Fig. 1 (a) Hydrothermal reactor to synthesize sugarcane bagasse-based biochar, rice husk-based biochar, and sawdust-based biochar) (b) Rotary shaker for petroleum spills adsorption

After 24 hours, the hydrothermal reactor was cooled and the precipitate containing magnetized biochar then washed with distilled water 3 times, followed by drying at 60°C for 4 hours under vacuum conditions. Biochar based on the raw material named sugarcane bagasse-based biochar, rice husk-based biochar, and sawdust-based biochar.

2.2.2. Characterizations

Biochar samples were characterized by using several analytical tools, including Scanning Electron Microscopy-Energy Dispersive X-Ray (SEM-EDX) JEOL JSM-6510LA for surface area and element composition observation; X-Ray Diffractometer (SHIMADZU X-Ray Diffraction (XRD)-7000) for crystal structure investigation; and Fourier transform infrared spectroscopy (FTIR) PerkinElmer spectrum IR 10.6.1 in the wavenumber range of 400 - 4000 cm^{-1} for the functional groups study. Instrument Autosorb iQ Station 1 was used for analysis The Brunauer, Emmett, and Teller (BET) adsorption isotherms and Barrett–Joyner–Halenda (BJH) pore size distribution. N_2 adsorption and desorption isotherm was measured at 77.35 K.

2.2.3. Petroleum Spill Adsorption

The effectiveness of biochar in absorbing petroleum spills was analysed by observing the adsorption capacity of biochar on crude oil on the surface of synthetic seawater. Materials that need to be prepared for the adsorption test include sugarcane bagasse-based biochar, rice husk-based biochar, sawdust-based biochar, crude oil, and synthetic seawater which have previously been prepared using distilled water, NaCl and KCL in a certain ratio. The experiment was carried out on an Erlenmeyer containing 200 mL of synthetic seawater, and 1 g of petroleum. The mixture was stirred and further processed with the addition of 4 g of biochar. Then Erlenmeyer with the solution was placed on a rotary shaker for 60 minutes. The speed of the rotary shaker was set so that the process can run at speed 150 rpm. Furthermore, biochar after the adsorption process is filtered and dried for 144 hours under atmospheric conditions and then weighed. The water adsorption ability of biochar was not considered in all experiments. The adsorption capacity of biochar in adsorbing oil spills and the adsorption effectiveness can be calculated using the following equation:

$$S = \frac{W_f - W_i}{W_i} \quad (1)$$

$$R\% = \frac{W_f - W_i}{W_o} \times 100\% \quad (2)$$

Where S is biochar adsorption capacity ($g.g^{-1}$), W_f is the dried weight of biochar after adsorption, W_i is the initial weight of biochar and W_o is the initial weight of petroleum that added to the system. R shows the effectiveness of biochar in adsorbing oil spills in percent.

3. Result and Discussion

3.1 Visual Characterizations of Biochar

The visual appearance of biochar with different raw materials can be seen in Fig. 2 (a), (b), (c). The resulting biochar was processed with the same treatment using the hydrothermal method, resulting in a different physical appearance. Biochar made from sawdust will produce black biochar powder, while biochar made from rice husk and sugarcane bagasse will produce a color that resembles the color of the raw material, which is brown. Based on these results, it can be concluded that the color of the raw materials used in biochar synthesis with the hydrothermal method affects the color of the synthesized biochar.

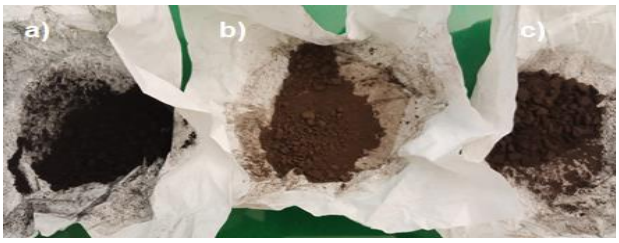

Fig. 2 Biochar from agricultural waste synthesized by hydrothermal method (a) sawdust-based biochar (b) rice husk-based biochar (c) sugarcane bagasse-based biochar

3.2 *Physical and Chemical Characterizations of Biochar*

The structure morphology and element compositions of sugarcane bagasse-based biochar, rice husk-based biochar, and sawdust-based biochar were analyzed using Scanning Electron Microscope and Energy Dispersive X-Ray **(**SEM**-**EDX) and the result presented in Fig. 3 (a), (b), and (c), respectively.

In the analysis of the Scanning Electron Microscope (SEM) an electron microscope is used which will produce an image of the sample by scanning the surface with a focused electron beam with a magnification of a certain scale. The electrons interact with atoms in the sample, generating various signals that contain information about the surface topography and composition of the sample. The Scanning Electron Microscope (SEM) images show the rough surface of all samples with various types of pores in the surface. The pores on the surface have different sizes and are distributed unevenly. Biochar derived from sugarcane bagasse (sugarcane bagasse-based biochar) is observed to have relatively small pores, while biochar originated from sawdust (sawdust-based biochar) tends to have moderate pores. The porous surface with a larger diameter of pores and higher numbers of pores were observed in biochar derived from rice husk (rice husk-based biochar). Elemental analysis for knowing element compositions on biochar was conducted by an Energy Dispersive X-Ray JEOL JSM-6510LA instrument with an energy range 0-20 keV. The analysis result is presented on Table 1 and the graph can be seen on Fig.3.

Energy Dispersive X-Ray Analysis (EDX) uses the main principle that characterization ability is largely due to the basic principle that each element has a unique atomic structure that allows for a unique set of peaks in its electromagnetic emission spectrum. The element analysis showed that the major composition of biochar whether sugarcane bagasse-based biochar, rice husk-based biochar, and sawdust-based biochar consists of C and O with a percentage of 93.2% for sugarcane bagasse-based biochar and 99.93% for sawdust-based biochar. While rice husk-based biochar element composition only 75.19% dominated with C and O with additional silica compounds with higher percentage compared to others. The element contained in sugarcane bagasse-based biochar is C, O, Si, Cl, and Fe. Oxygen and silica can form SiO_2 compounds, whereas the interaction between oxygen and Fe resulting FeO compounds. Besides silica, rice husk-based biochar also contains Fe and a small amount of Al which can interact with oxygen to form Al_2O_3. Different things are shown by sawdust-based biochar that the main constituents are C and O, and a little amount of Na to form Na_2O and Al to form Al_2O_3. The result shows the attachment of magnetic compound was successfully conducted in sugarcane bagasse-based biochar and rice husk-based biochar surface area.

Table 1
Element compositions from Energy Dispersive X-Ray (EDX) analysis on sugarcane bagasse-based biochar, rice husk-based biochar, and sawdust-based biochar

Compositions (Mass %)	Sugarcane Bagasse-Based Biochar		Rice Husk-Based Biochar		Sawdust-Based Biochar	
	pure	oxide	pure	oxide	pure	oxide
C	51.96	83.41	44.54	54,73	59.86	99.74
O	41.24	-	30.65	-	40.07	-
Si	1.18	4.25	7.16	18,17	-	-
Cl	0.23	0.39	0.29	0.35	-	-
Fe	5.39	11.95	17.16	26.28	-	-
Na	-	-	-	-	0.01	0.01
Al	-	-	0.21	0.48	0.07	0.25
TOTAL	100	100	100	100	100	100

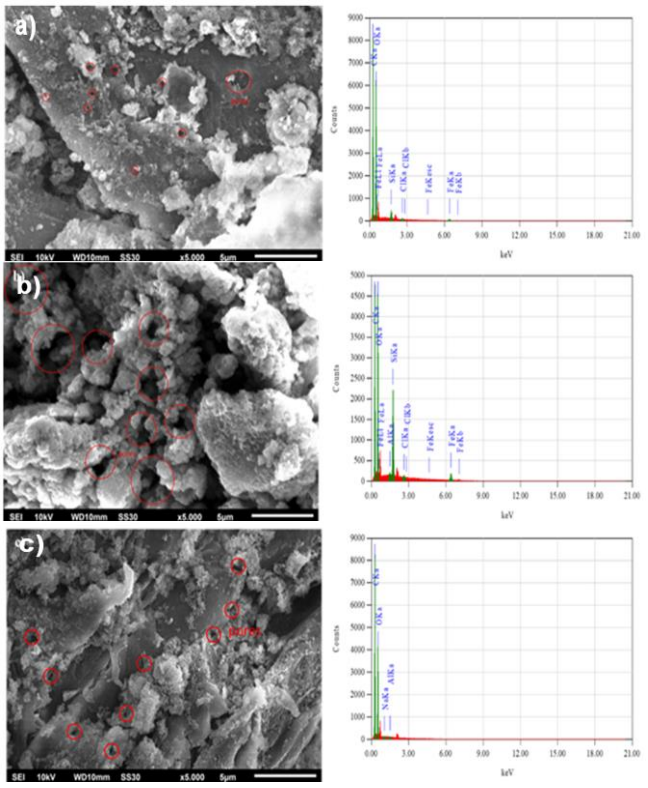

Fig. 3 Scanning Electron Microscope and Energy Dispersive X-Ray of (a) sugarcane bagasse-based biochar (b) rice husk-based biochar (c) sawdust-based biochar

The X-Ray Diffraction (XRD) results of all samples synthesized from bagasse, risk husk, and sawdust are shown in Fig. 4. The basic principle of XRD is to diffraction light through a crystal gap. Diffraction of light by this lattice or crystal can occur if the diffraction comes from a radius that has a wavelength equivalent to the distance between atoms. The X-Ray Diffraction (XRD) pattern of all the samples indicated the synthesized biochar was completely amorphous by the featureless diffractograms by means of amorphous carbon. The hydrothermal process was not significantly affected the crystallinity of the product. The appearance of a diffuse maximum for rice husk-based biochar at 23° indicate for amorphous silica (Asadi Zeidabadi *et al.*, 2018), whereas a diffuse maximum for sugarcane bagasse-based biochar at 66.82° and sawdust-based biochar at 21.8° is denoted as the graphitic structure of carbon which is the dominant element of sample (Armynah *et al.*, 2018; Cai *et al.*, 2019).

Fourier transform infrared spectroscopy (FTIR) spectra of biochar from bagasse, rice husk, and sawdust is presented in Fig. 5. FTIR analysis needs to be carried out to determine the existence of functional groups that have an important role in the pollutant adsorption process. Based on analysis result, all sample almost has the same functional group but varied in percentage of transmittance. The highest percentage of absorbance was observed in the rice husk-based biochar spectra, followed by sugarcane bagasse-based biochar and sawdust-based biochar. The more absorbance in Fourier transforms infrared spectroscopy (FTIR) spectra indicated the presence of more specific bond numbers in the sample at a specific wavelength. Meanwhile, the functional group consist of hydroxyl groups (-OH), asymmetric and symmetric stretching (C-H stretching), carbonyl (C=O stretching) and alkoxy stretching vibration (C-O stretching).

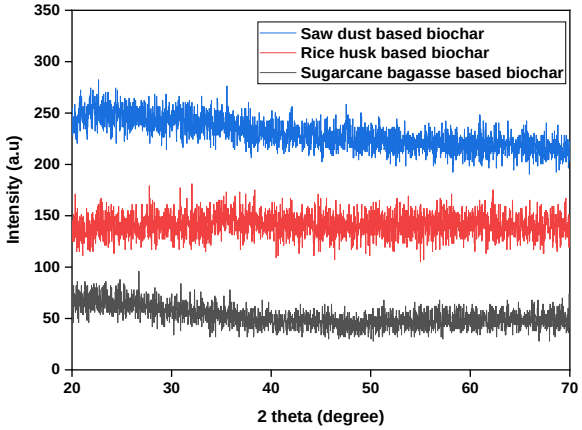

Fig. 4 X-Ray Diffraction (XRD) pattern of different biochar that synthesizes from bagasse (sugarcane bagasse-based biochar), rice husk (rice husk-based biochar), and sawdust (sawdust-based biochar)

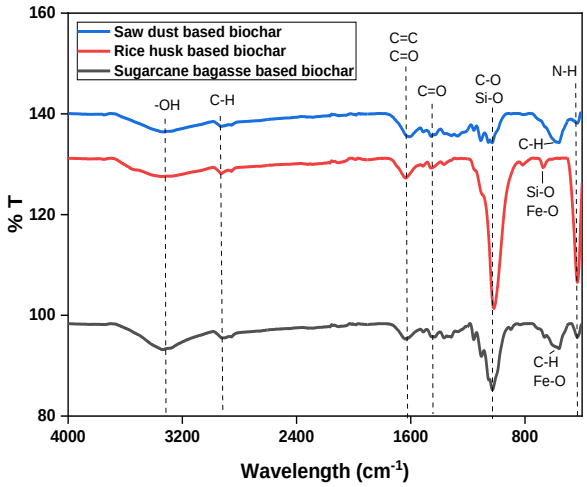

Fig. 5 FT-IR Spectra of biochar synthesizes from bagasse (sugarcane bagasse-based biochar), rice husk (rice husk-based biochar), and sawdust (sawdust-based biochar)

Table 2
Functional groups on sugarcane bagasse-based biochar, rice husk-based biochar, and sawdust-based biochar based on wavenumber (cm^{-1})

Wavenumber (cm^{-1})			Annotation
Bagasse-Based Biochar	Rice Husk-Based Biochar	Sawdust-Based Biochar	
432.98	432.98	434.01	N-H stretching vibration
561.86		562.40	C-H bending from aromatic ring or Fe-O stretching vibration
-	672.5	-	Si-O or Fe-O stretching vibration
1027.71	1018.37	1029.64	(C-O) stretching vibrations ester and aliphatic ether or Si-O stretching vibration
1433.37	1457.16	1456.48	(C=O) stretching vibrations
1636.02	1635.62	1609.93	(C=C) and (C=O) stretching compounds
2916.51	2927.58	2928.29	(C-H) stretching aliphatic compounds (CH_3, CH_2)
3335.94	3342.73	3337.72	(-OH) stretching vibrations

The stretching vibrations of hydroxyl group showed the broad intense signal around 3335 cm^{-1} (Cai *et al.*, 2019). The band around 2916 cm^{-1} ascribed to the symmetric and asymmetric stretching aliphatic compounds CH_3 and CH_2 (C-H stretching) (Creamer *et al.*, 2014; El Gheriany *et al.*, 2020; H. Zhang & Hay, 2020). The aromatic rings (C=C bond) and carbonyl group (C=O stretching) visible approximately 1635 cm^{-1} (AlAmeri *et al.*, 2019). The signal around 1433 cm^{-1} corresponded with C=O stretching vibration (Duan *et al.*, 2021). The band around 1027 cm^{-1} can be contributed to alkoxy C-O stretching vibrations ester and aliphatic ether or Si-O stretching vibration due to silica content on sugarcane bagasse-based biochar and rice husk-based biochar (El Gheriany *et al.*, 2020; Lee *et al.*, 2013). Si-O and Fe-O stretching also showed at 672,5 cm^{-1} for rice husk-based biochar (He *et al.*, 2017; Lee *et al.*, 2013). Moreover C-H bending from aromatic ring or Fe-O stretching seen around 561 cm^{-1} (Ahmed *et al.*, 2020; Cai *et al.*, 2019). The existence of amine group for hexamethyl diamine (HDA) also attributed to N-H stretching vibration at 432 cm^{-1} (Duan *et al.*, 2021). All Fourier transform infrared spectroscopy (FTIR) data can be resumed on Table 2.

3.2 Oil sorption Capacity

To observe the adsorption capacity of biochar, an experiment was carried out by adding biochar to an Erlenmeyer containing synthetic seawater and oil spills. The adsorbed petroleum is obtained by weighing the biochar that has undergone the adsorption process for 60 minutes and removal of water content with slow atmospheric drying for 144 hours. Capacity and effectiveness of adsorption can be presented in the Fig. 6.

Figure 6 shows that all sample possesses good adsorption capacity. Bagasse-based biochar can adsorb as much as 81% of petroleum spills. Meanwhile rice husk-based biochar has better adsorption ability, where this adsorbent is able to adsorb petroleum spill as much as 84%. Saw dust-based biochar also has good adsorption ability, where the adsorbed petroleum spill is 70%, but this value is not better when compared to bagasse-based biochar and rice husk-based biochar. The adsorption ability of biochar and the formation of magnetized biochar is inseparable from the addition of HDA and $FeCl_3.6H_2O$. Adding hexamethyl diamine (HDA) enhance active side on surface of magnetized biochar, so the capability to adsorb adsorbate increase, besides $FeCl_3.6H_2O$ also has a role to form iron oxide. By hydrothermal process, iron oxide advances the size of biochar pores (H. Zhang & Hay, 2020). This condition has been proven by Cai *et al*, that compare the adsorption capacity of biochar with including HDA and $FeCl_3.H_2O$ in the synthesis process. The maximum adsorption capacity was obtained when biochar synthesize using both reagents than only adding HDA without $FeCl_3.H_2O$ (Cai *et al.*, 2019) or without the addition of both reagents at all. The formation mechanism of magnetized biochar can be explained as follow:

$$2Fe^{3+} + 3H_2N-(CH_2)_6-NH_2 + 6H_2O \rightarrow 2Fe(OH)_3 + {}^{3+}H_3N-(CH_2)_6-NH_3^+ \quad (1)$$

$$2Fe(OH)_3 \xrightarrow{\text{hydrothermal}} \gamma Fe_2O_3 + 3H_2O \quad (2)$$

$$R-C=O + 3H_2N-(CH_2)_6-NH_2 \xrightarrow{\text{hydrothermal}} R-C=N-(CH_2)_6-NH_2(\text{Schiffbase}) + H_2O \quad (3)$$

$$R-COOH + 3H_2N-(CH_2)_6-NH_2 \xrightarrow{\text{hydrothermal}} R-CONH(CH_2)_6-NH_2 + H_2O \quad (4)$$

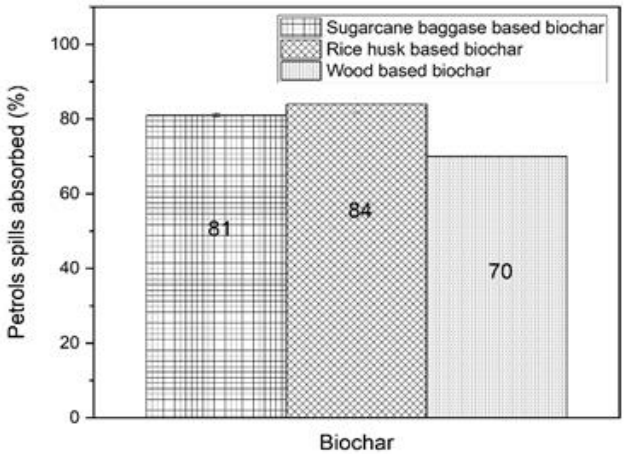

Fig. 6 Absorption capacity of (a) sugarcane bagasse-based biochar, (b) rice husk-based biochar, (c) sawdust-based biochar in petroleum spills absorption application

In synthesized biochar, hexamethyl diamine (HDA) was added in the solution to bring out alkaline conditions that triggered hydrolysis Fe^{3+} to form $Fe(OH)_3$ on the surface of the biomass. Throughout the hydrothermal process, $Fe(OH)_3$ vastly dehydrates into ɤ-Fe_2O_3 and some of the cellulose and hemicellulose from the waste biomass hydrolyzes forming saccharides, which then dehydrate into molecules (R-C=O) (Kıvancc Aydıncak, Tugrul Yumak, Ali Sınag, 2012; Qin *et al.*, 2022; Ryu *et al.*, 2010). Following the Mannich reaction, the two activated hydrogens of hexamethyl diamine (HDA) (H_2N-$(CH_2)_6$-NH_2) and R-C=O generate a Schiff base, which can make C=N. The remaining portion of the biomass simultaneously undergoes hydrolysis, dehydration, and condensation to form aromatic-structured biochar with many carboxyl groups (R-COOH) and hydroxyl groups (R-OH) (Kıvancc Aydıncak, Tugrul Yumak, Ali Sınag, 2012). Afterward, the R-COOH and hexamethyl diamine (HDA) undergo a condensation process to create amide (N-C=O). Therefore, carbonization, magnetization and amino-functionalization as one step simultaneously process could be realized (Cai *et al.*, 2019).

Rice husk-based biochar possesses excellent adsorption capacity than sugarcane bagasse-based biochar and sawdust-based biochar. The Adsorption capacity of rice husk-based biochar is 84% with an effectiveness of 0.21 g/g within 60 mins. Referring to the SEM-EDX results, rice husk-based biochar has a more porous surface that is unevenly distributed than sugarcane bagasse-based biochar and sawdust-based biochar. In addition, this sample also contains silica and iron with a higher composition than the other samples. These two elements can interact with oxygen to form functional groups that increase the active site on biochar surface so it can adsorb more petroleum spill.

Table 3
The Brunauer, Emmett, and Teller (BET) and Barrett–Joyner–Halenda (BJH) analysis result of sugarcane bagasse-based biochar, rice husk-based biochar, and sawdust-based biochar

Sample	Surface area (m^2/g)	Total pore volume (cc/g)	Average pore diameter (nm)
Sugarcane bagasse-based biochar	51.286	0.2077	16.196
Rice husk-based biochar	83.651	0.3331	15.926
Sawdust-based biochar	92.901	0.3883	16.718

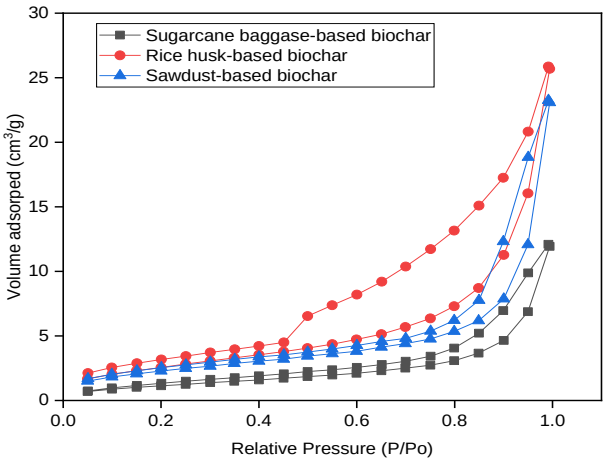

Fig. 7. N_2 adsorption and desorption isotherm of sugarcane bagasse-based biochar, rice husk-based biochar, sawdust-based biochar and pore size distribution of biochar

The Brunauer, Emmett, and Teller (BET) adsorption isotherms models and Barrett–Joyner–Halenda (BJH) pore size distribution curve is represented in Fig. 7, and a summary of the result is shown in Table 3. N_2 adsorption and desorption isotherm was measured at 77.35 K. Surface area is an important morphological characterization of solid materials, especially in pore structures. Pores with d_{pore} < 2 nm are classified as micropores, whereas pores with sizes between 2 and 50 nm are mesopores, and d_{pore} > 50 nm are macropores. Based on the data presented in Table 3, all samples are categorized as mesopores due to pore size around 15 to 16 nm. The IUPAC categorizes the adsorption isotherms into six types (isotherm types I to VI) and the hysteresis patterns into four types (hysteresis loops H1 to H4), which are both commonly used to characterize the physisorption mechanisms of porous solids.

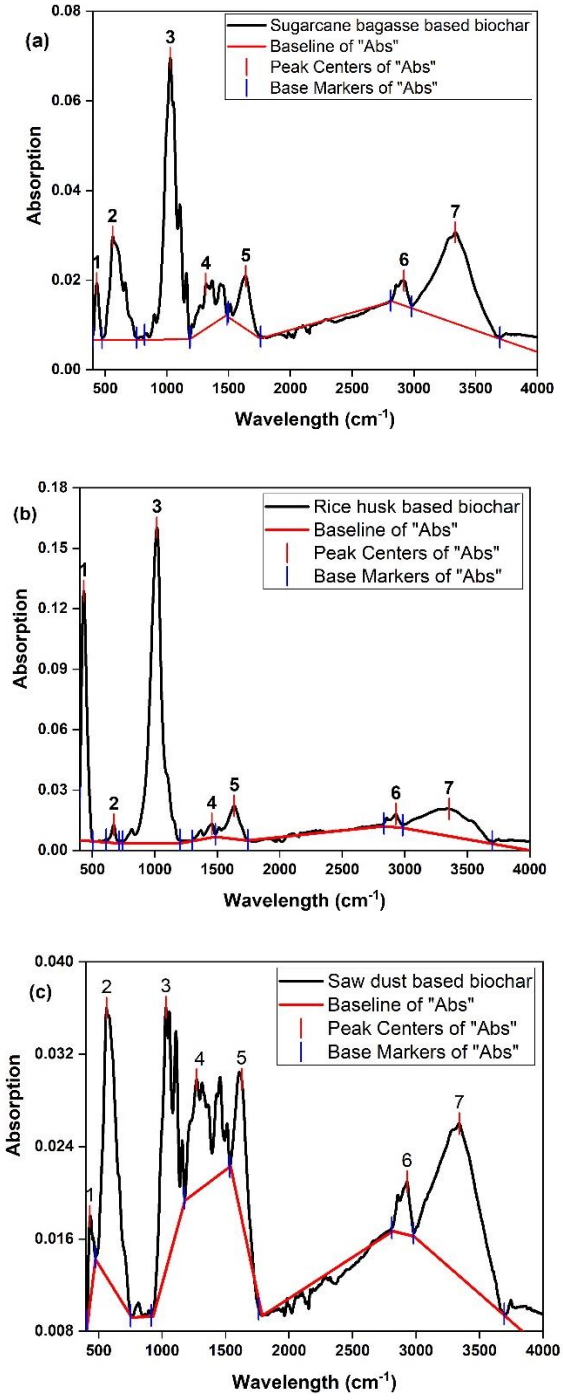

Fig. 8. Area functional group of (a) sugarcane bagasse- based biochar, (b) rice husk-based biochar, (c) sawdust-based biochar

Table 4
Area functional group of sugarcane bagasse- based biochar, rice husk-based biochar, sawdust-based biochar

Functional group	sugarcane bagasse- based biochar		rice husk-based biochar		sawdust-based biochar	
	Peak No.	Area	Peak No.	Area	Peak No.	Area
N-H	1	0.494	1	6.230	1	0.274
C-H	2	2.928		-	2	2.949
Si-O	-	-	2	0.3862	-	-
C-O / Si-O	3	7.7301	3	18.132	3	2.7282
C=O	4	1.7490	4	0.64	4	2.0738
C=C / C=O	5	1.3271	5	1.9507	5	1.1736
C-H	6	0.5564	6	0.5850	6	0.4516
-OH	7	6.7672	7	6.0415	7	4.8901
Total peak area		21.5528		33.9673		14.5416

The N_2 isotherm of biochar shows a type IV isotherm, where the interaction between absorbent mesopore surface and gas molecules induces capillary condensation that causes the desorption path will be different from the adsorption path, creating a hysteresis loop. The type of loop is generally related to pore shape. According to the N_2 adsorption and desorption isotherm, the hysteresis loop for this study follows type H3 (Bardestani *et al.*, 2019). From Table 3, it can be shown that the largest surface area and total pore volume owned by sawdust-based biochar, followed by rice husk-based biochar, and the smallest is sugarcane bagasse-based biochar. This condition is inversely proportional to the adsorption capacity, where rice husk-based biochar has the best adsorption capacity compared to the others. The adsorption capacity of a material is not only influenced by the surface area and pore volume. An excellent adsorption ability also can be attained when the materials have a large content of oxygen functional groups. Excellent biochar absorption capacity is also supported by the existence of a functional group. The Area of a functional group can be calculated using Origin Pro 2018, the graph and resulting data are shown on Fig.8 and Table 4. In determining the area of functional groups using Origin software, the first step is to convert transmittance data into adsorption data. Then determine the baseline on the graph that has been made. Baseline correction is an important pre-processing technique used to separate true spectroscopic signals from interference effects or remove background effects, stains or traces of compounds. The next step is selecting the method to be used in peak fitting. The peaks on the graphs are determined and then integrated. The software will automatically calculate the area of functional groups at each peak. According to Fig. 8 and data from Table 4, the type of functional group contained in all sample is almost the same. The significant difference in functional group area is found in the N-H and Si-O that are found in the rice husk-based biochar. The existence of the N-functional group in biochar comes from the use of hexametyldiamine in the hydrothermal process. Hexamethyldiamine is an organic compound consisting of a hexamethylene hydrocarbon chain terminated with an amine functional group. In the presence of HDA, a condensation reaction occurs which produces N-functional groups in biochar according to the reactions that occur in equations (3) and (4). The existence of the N-functional group in sugarcane bagasse-based biochar and sawdust-based biochar is less due to the instability of these components during the reaction process thus they are easily decomposed to form other components such as NH_3 which is volatile. The fewer N-Functional groups that are formed, the smaller the area. The successful formation of the N-functional group in biochar is also influenced by several factors, one of which is the feedstock. Based on data by Leng *et al.* the more nitrogen contained in the biomass, the greater the nitrogen content in the biochar, thereby increasing the N-functional group and its area (Leng *et al.*, 2020). Several studies have shown data related to the ultimate analysis of feedstock and biochar. If it is compared between the two biomass, rice husk contains Nitrogen 1.2% w and sawdust contains less nitrogen, only 0.41% w. After it is synthesized, the nitrogen content in rice husk biochar is 0.81% while sawdust-based biochar is 0.56 % w (Abbas *et al.*, 2018; Chellappan *et al.*, 2018). Likewise for the Si-O which is the dominant functional group in rice husk-based biochar. Rice husk has quite a lot of silica content of 18.3% so the formation of SiO functional groups in the product will be more than the others. The more Si-O functional groups formed, the larger the area (Battegazzore *et al.*, 2014). Rice husk biochar contains 15-20% silica (Singh Karam *et al.*, 2022). Excellent capability of sample in absorption can be achieved when the materials owned large functional groups content which provides more active sites, so it can easier absorb the absorbate into the surface (Nguyen-Phan *et al.*, 2011). Based on the data above, it proves rice husk-based biochar has the capability to absorb petroleum spills in comparison to others because it possesses a wider functional group area, by means the availability of active site on the surface that has contact with absorbate is higher than sugarcane bagasse-based biochar and sawdust-based biochar.

4. Conclusion

Magnetic biochar has successfully been synthesized using sugarcane bagasse, and rice husk as raw material by hydrothermal method. This is based on the results of Scanning Electron Microscope and Energy Dispersive X-Ray **(**SEM**-**EDX) and also Fourier transform infrared spectroscopy (FTIR) analysis, where the two biochars contain iron oxide on their surface. The results of the X-Ray Diffraction (XRD) analysis showed that all biochar, both sugarcane-based biochar, rice husk-based biochar, and sawdust-based biochar, did not show any crystal formation so that all three were amorphous. Absorption capacity was observed using petroleum spills for 60 minutes. The results indicate that all samples can absorb petroleum spills with a percentage 81% for sugarcane bagasse-based biochar, 84% for rice husk-based biochar, and 70% for sawdust-based biochar. Based on The Brunauer, Emmett, and Teller (BET) adsorption isotherms models and Barrett–Joyner–Halenda (BJH), all samples are categorized as mesopores due to pore size around 15 to 16 nm. Rice husk-based biochar and sugarcane bagasse-based biochar have a smaller surface area than sawdust-based biochar, but have better adsorption ability. The adsorption ability of an adsorbent is not only influenced by surface area but also because it has a larger functional group area. Rice husk-based biochar has the largest functional group area compared to sugarcane bagasse- based biochar and sawdust based-biochar, so it has the best adsorption ability The addition of hexamethyl diamine (HDA) and $FeCl_3.6H_2O$ in the synthesis process also affects biochar adsorption capacity. The

best results are obtained with biochar derived from rice husk that is used to absorb petroleum spills as it has a larger functional group area and the excellent attachment of magnetic compound into the biochar surface to form magnetic biochar.

Acknowledgments

This research was financially supported by The Faculty of Engineering, Diponegoro University, Indonesia through Strategic Research Grant 2022.

Author Contributions: Dessy Ariyanti: Conceptualization, methodology, formal analysis, writing—original draft, I Nyoman Widiasa; supervision, resources, conceptualization, Marissa Widiyanti; writing—review and editing, project administration, validation, Dina Lesdantina; writing—review and editing, project administration, validation, Wei Gao: supervision, resources, conceptualization.

Funding: This research was funded by The Faculty of Engineering, Diponegoro University, Indonesia through Strategic Research Grant 2022 with research implementation agreement letter No. 3178 / S / kimia / 10 / UN7.5.3.2 / PP / 22.

Conflicts of Interest: The authors declare no conflict of interest in conducting research and writing this article. All research results and interpretations are in accordance with actual conditions and there is no intervention from any party.

References

Abbas, Q., Liu, G., Yousaf, B., Ali, M. U., Ullah, H., Munir, M. A. M., & Liu, R. (2018). Contrasting effects of operating conditions and biomass particle size on bulk characteristics and surface chemistry of rice husk derived-biochars. *Journal of Analytical and Applied Pyrolysis*, *134*, 281–292. https://doi.org/10.1016/j.jaap.2018.06.018

Ahmed, A., Abu Bakar, M. S., Sukri, R. S., Hussain, M., Farooq, A., Moogi, S., & Park, Y. K. (2020). Sawdust pyrolysis from the furniture industry in an auger pyrolysis reactor system for biochar and bio-oil production. *Energy Conversion and Management*, *226*, 113502. https://doi.org/10.1016/j.enconman.2020.113502

AlAmeri, K., Giwa, A., Yousef, L., Alraeesi, A., & Taher, H. (2019). Sorption and removal of crude oil spills from seawater using peat-derived biochar: An optimization study. *Journal of Environmental Management*, *250*, 109465. https://doi.org/10.1016/j.jenvman.2019.109465

Armynah, B., Djafar, Z., & Piarah, W. H. (2018). Analysis of Chemical and Physical Properties of Biochar from Rice Husk Biomass. *J. Phys.: Conf. Ser.* 979, 012038. https://doi.org/10.1088/1742-6596/979/1/012038

Asadi Zeidabadi, Z., Bakhtiari, S., Abbaslou, H., & Ghanizadeh, A. R. (2018). Synthesis, characterization and evaluation of biochar from agricultural waste biomass for use in building materials. *Construction and Building Materials*, *181*, 301–308. https://doi.org/10.1016/j.conbuildmat.2018.05.271

Aydincak, K., Yumak, T., Sınağ, A., & Esen, B. (2012). Synthesis and Characterization of Carbonaceous Materials from Saccharides (Glucose and Lactose) and Two Waste Biomasses by Hydrothermal Carbonization. *Industrial & Engineering Chemistry Research,* 51, 9145-9152. https://doi.org/10.1021/ie301236h

Bardestani, R., Patience, G. S., & Kaliaguine, S. (2019). Experimental methods in chemical engineering: specific surface area and pore size distribution measurements—BET, BJH, and DFT. *Canadian Journal of Chemical Engineering*, *97*(11), 2781–2791. https://doi.org/10.1002/cjce.23632

Battegazzore, D., Bocchini, S., Alongi, J., & Frache, A. (2014). Rice husk as bio-source of silica: Preparation and characterization of PLA-silica bio-composites. *RSC Advances*, 4(97). https://doi.org/10.1039/c4ra05991c

Cai, W., Wei, J., Li, Z., Liu, Y., Zhou, J., & Han, B. (2019). Preparation of amino-functionalized magnetic biochar with excellent adsorption performance for Cr(VI) by a mild one-step hydrothermal method from peanut hull. *Colloids and Surfaces A: Physicochemical and Engineering Aspects*, *563*, 102–111. https://doi.org/10.1016/j.colsurfa.2018.11.062

Chellappan, S., Nair, V., Sajith, V., & Aparna, K. (2018). Synthesis, optimization and characterization of biochar based catalyst from sawdust for simultaneous esterification and transesterification. *Chinese Journal of Chemical Engineering*, 2654–2663. https://doi.org/10.1016/j.cjche.2018.02.034

Creamer, A. E., Gao, B., & Zhang, M. (2014). Carbon dioxide capture using biochar produced from sugarcane bagasse and hickory wood. *Chemical Engineering Journal*, 249, 174–179. https://doi.org/10.1016/j.cej.2014.03.105

Duan, H., Lyu, H., Shen, B., Tian, J., Pu, X., Wang, F., & Wang, X. (2021). Superhydrophobic-superoleophilic biochar-based foam for high-efficiency and repeatable oil-water separation. *Science of the Total Environment*, *780*, 146517. https://doi.org/10.1016/j.scitotenv.2021.146517

Duke, N. C. (2016). Oil spill impacts on mangroves: Recommendations for operational planning and action based on a global review. *Marine Pollution Bulletin*, 109(2), 700–715. https://doi.org/10.1016/j.marpolbul.2016.06.082

El Gheriany, I. A., Ahmad El Saqa, F., Abd El Razek Amer, A., & Hussein, M. (2020). Oil spill sorption capacity of raw and thermally modified orange peel waste. *Alexandria Engineering Journal*, *59*(2), 925–932. https://doi.org/10.1016/j.aej.2020.03.024

Graham, L. J., Hale, C., Maung-douglass, E., & Sempier, S. (2010). Chemical dispersants and their role in oil spill response (2016a). Available at: https://protect-eu.mimecast.com/s/4-PVCOgDgsA4O0oUPQiLn?domain=masgc.org

Gurav, R., Bhatia, S. K., Choi, T. R., Choi, Y. K., Kim, H. J., Song, H. S., Park, S. L., Lee, H. S., Lee, S. M., Choi, K. Y., & Yang, Y. H. (2021). Adsorptive removal of crude petroleum oil from water using floating pinewood biochar decorated with coconut oil-derived fatty acids. *Science of the Total Environment*, 781, 146636. https://doi.org/10.1016/j.scitotenv.2021.146636

He, S., Zhong, L., Duan, J., Feng, Y., Yang, B., & Yang, L. (2017). Bioremediation of wastewater by iron Oxide-Biochar nanocomposites loaded with photosynthetic bacteria. *Frontiers in Microbiology*, 8, 1–10. https://doi.org/10.3389/fmicb.2017.00823

Helle, I., Mäkinen, J., Nevalainen, M., Afenyo, M., & Vanhatalo, J. (2020). Impacts of Oil Spills on Arctic Marine Ecosystems: A Quantitative and Probabilistic Risk Assessment Perspective. *Environmental Science and Technology*, *54*(4), 2112–2121. https://doi.org/10.1021/acs.est.9b07086

Honda, M., & Suzuki, N. (2020). Toxicities of polycyclic aromatic hydrocarbons for aquatic animals. *International Journal of Environmental Research and Public Health*, *17*(4). https://doi.org/10.3390/ijerph17041363

Institute, B. (2022). *Tumpahan Minyak di Laut dan Langkah Antisipasi Pemerintah Indonesia | BHR Institute*. https://bhrinstitute.id/tumpahan-minyak-di-laut-dan-langkah-antisipasi-pemerintah-indonesia/

ITOPF. (2022). *Tanker spill statistics 2021*. https://www.itopf.org/news-events/news/tanker-spill-statistics-2021/

KKP. (2022). *KKP |Kementerian Kelautan dan Perikanan*. https://kkp.go.id/djprl/p4k/page/2626-tumpahan-minyak-oil-spill

Lee, T., Othman, R., & Yeoh, F. Y. (2013). Development of photoluminescent glass derived from rice husk. *Biomass and Bioenergy*, 59, 380–392. https://doi.org/10.1016/j.biombioe.2013.08.028

Leng, L., & Huang, H. (2018). An overview of the effect of pyrolysis process parameters on biochar stability. *Bioresource Technology*, *270*(September), 627–642. https://doi.org/10.1016/j.biortech.2018.09.030

Leng, L., Xu, S., Liu, R., Yu, T., Zhuo, X., Leng, S., Xiong, Q., & Huang, H. (2020). Nitrogen containing functional groups of biochar: An overview. *Bioresource Technology*, *298*, 122286. https://doi.org/10.1016/j.biortech.2019.122286

Li, W., Dang, Q., Brown, R. C., Laird, D., & Wright, M. M. (2017). The impacts of biomass properties on pyrolysis yields, economic and environmental performance of the pyrolysis-bioenergy-biochar platform to carbon negative energy. *Bioresource Technology*, *241*, 959–968. https://doi.org/10.1016/j.biortech.2017.06.049

Madhubashani, A. M. P., Giannakoudakis, D. A., Amarasinghe, B. M. W.

P. K., Rajapaksha, A. U., Pradeep Kumara, P. B. T., Triantafyllidis, K. S., & Vithanage, M. (2021). Propensity and appraisal of biochar performance in removal of oil spills: A comprehensive review. *Environmental Pollution*, *288*, 117676. https://doi.org/10.1016/j.envpol.2021.117676

Nguyen-Phan, T. D., Pham, V. H., Shin, E. W., Pham, H. D., Kim, S., Chung, J. S., Kim, E. J., & Hur, S. H. (2011). The role of graphene oxide content on the adsorption-enhanced photocatalysis of titanium dioxide/graphene oxide composites. *Chemical Engineering Journal*, *170*(1), 226–232. https://doi.org/10.1016/j.cej.2011.03.060

Ouyang, D., Chen, Y., Yan, J., Qian, L., Han, L., & Chen, M. (2019). Activation mechanism of peroxymonosulfate by biochar for catalytic degradation of 1,4-dioxane: Important role of biochar defect structures. *Chemical Engineering Journal*, *370*, 614–624. https://doi.org/10.1016/j.cej.2019.03.235

Piperopoulos, E., Calabrese, L., Mastronardo, E., Proverbio, E., & Milone, C. (2020). Sustainable Reuse of Char Waste for Oil Spill Recovery Foams. *Water, Air, and Soil Pollution*, *231*(6). https://doi.org/10.1007/s11270-020-04671-2

Qin, F., Zhang, C., Zeng, G., Huang, D., Tan, X., & Duan, A. (2022). Lignocellulosic biomass carbonization for biochar production and characterization of biochar reactivity. *Renewable and Sustainable Energy Reviews*, *157*, 112056. https://doi.org/10.1016/j.rser.2021.112056

Rajabi, H., Hadi Mosleh, M., Prakoso, T., Ghaemi, N., Mandal, P., Lea-Langton, A., & Sedighi, M. (2021). Competitive adsorption of multicomponent volatile organic compounds on biochar. *Chemosphere*, *283*. https://doi.org/10.1016/j.chemosphere.2021.131288

Ryu, J., Suh, Y. W., Suh, D. J., & Ahn, D. J. (2010). Hydrothermal preparation of carbon microspheres from mono-saccharides and phenolic compounds. *Carbon*, *48*(7), 1990–1998. https://doi.org/10.1016/j.carbon.2010.02.006

Sabir, S. (2015). Approach of cost-effective adsorbents for oil removal from oily water. *Critical Reviews in Environmental Science and Technology*, *45*(17), 1916–1945. https://doi.org/10.1080/10643389.2014.1001143

Singh, H., Bhardwaj, N., Arya, S. K., & Khatri, M. (2020). Environmental impacts of oil spills and their remediation by magnetic nanomaterials. *Environmental Nanotechnology, Monitoring and Management*, *14*, 100305. https://doi.org/10.1016/j.enmm.2020.100305

Singh Karam, D., Nagabovanalli, P., Sundara Rajoo, K., Fauziah Ishak, C., Abdu, A., Rosli, Z., Melissa Muharam, F., & Zulperi, D. (2022). An overview on the preparation of rice husk biochar, factors affecting its properties, and its agriculture application. *Journal of the Saudi Society of Agricultural Sciences*, *21*(3), 149–159. https://doi.org/10.1016/j.jssas.2021.07.005

Subrati, A., Mondal, S., Ali, M., Alhindi, A., Abdala, A., Reinalda, D., & Alhassan, S. M. (2017). Developing Hydrophobic Graphene Foam for Oil spill Cleanup. *Industrial & Engineering Chemistry Research*, 56, 6945-6951. https://doi.org/10.1021/acs.iecr.7b00716.

Tao, T., Li, G., He, Y., & Yang, X. (2019). 3-D magnetic graphene balls as sorbents for cleaning oil spills. *Nanomaterials and Nanotechnology*, *9*, 1–7. https://doi.org/10.1177/1847980419857373

Wei, Z., Wang, J. J., Meng, Y., Li, J., Gaston, L. A., Fultz, L. M., & DeLaune, R. D. (2020). Potential use of biochar and rhamnolipid biosurfactant for remediation of crude oil-contaminated coastal wetland soil: Ecotoxicity assessment. *Chemosphere*, *253*, 126617. https://doi.org/10.1016/j.chemosphere.2020.126617

Wu, J., Yang, J., Huang, G., Xu, C., & Lin, B. (2020). Hydrothermal carbonization synthesis of cassava slag biochar with excellent adsorption performance for Rhodamine B. *Journal of Cleaner Production*, *251*, 119717. https://doi.org/10.1016/j.jclepro.2019.119717

Yaashikaa, P. R., Kumar, P. S., Varjani, S., & Saravanan, A. (2020). A critical review on the biochar production techniques, characterization, stability and applications for circular bioeconomy. *Biotechnology Reports*, *28*, e00570. https://doi.org/10.1016/j.btre.2020.e00570

Yi, Y., Huang, Z., Lu, B., Xian, J., Tsang, E. P., Cheng, W., Fang, J., & Fang, Z. (2020). Magnetic biochar for environmental remediation: A review. *Bioresource Technology*, *298*(September 2019). https://doi.org/10.1016/j.biortech.2019.122468

Yuewen, D., & Adzigbli, L. (2018). Assessing the Impact of Oil Spills on Marine Organisms. *Journal of Oceanography and Marine Research*, 06(01). https://doi.org/10.4172/2572-3103.1000179

Zhang, B., Matchinski, E. J., Chen, B., Ye, X., Jing, L., & Lee, K. (2018). Marine oil spills-oil pollution, sources and effects. In *World Seas: An Environmental Evaluation Volume III: Ecological Issues and Environmental Impacts* (Second Edi). Elsevier Ltd. https://doi.org/10.1016/B978-0-12-805052-1.00024-3

Zhang, H., & Hay, A. G. (2020). Magnetic biochar derived from biosolids via hydrothermal carbonization: Enzyme immobilization, immobilized-enzyme kinetics, environmental toxicity. *Journal of Hazardous Materials*, 384, 121272. https://doi.org/10.1016/j.jhazmat.2019.121272

© 2023. The Author(s). This article is an open access article distributed under the terms and conditions of the Creative Commons Attribution-ShareAlike 4.0 (CC BY-SA) International License (http://creativecommons.org/licenses/by-sa/4.0/)